RI 8860

PLEASE DO NOT REMOVE FROM LIBRARY

Bureau of Mines Report of Investigations/1984

Low-Chromium Heat-Resisting Ferritic Alloys Strengthened by the Chi Phase

By M. L. Glenn and J. S. Dunning

UNITED STATES DEPARTMENT OF THE INTERIOR

Report of Investigations 8860

Low-Chromium Heat-Resisting Ferritic Alloys Strengthened by the Chi Phase

By M. L. Glenn and J. S. Dunning

UNITED STATES DEPARTMENT OF THE INTERIOR
William P. Clark, Secretary

BUREAU OF MINES
Robert C. Horton, Director

Library of Congress Cataloging in Publication Data:

Glenn, M. L. (Max L.)

Low-chromium heat-resisting ferritic alloys strengthened by the chi phase.

(Report of investigations ; 8860)

Bibliography: p. 16-18.

Supt. of Docs. no.: I 28.23:8860.

1. Chromium-iron alloys. 2. Heat resistant alloys. 3. Precipitation hardening. 4. Intermetallic compounds. I. Dunning, J. S. II. Title. III. Series: Report of investigations (United States. Bureau of Mines) ; 8860.

TN23.U43 [TN799.C5] 622s [669'.951] 83-600362

CONTENTS

ILLUSTRATIONS

TABLES

UNIT OF MEASURE ABBREVIATIONS USED IN THIS REPORT

at. pct	atomic percent	lb	pound
°C	degree Celsius	mg	milligram
g	gram	mg/cm^3	milligram per cubic centimeter
g/cm^3	gram per cubic centimeter	min	minute
gpL	gram per liter	mm	millimeter
h	hour	pct	percent
in	inch	V	volt
$in/in \cdot min^{-1}$	inch per inch per minute	wt pct	weight percent
kg	kilogram		

LOW-CHROMIUM HEAT-RESISTING FERRITIC ALLOYS STRENGTHENED BY THE CHI PHASE

By M. L. Glenn [1] and J. S. Dunning [1]

ABSTRACT

The Bureau of Mines is conducting research on substitutes for chromium-containing alloys in order to conserve imported critical and strategic materials. Part of this research concentrates on finding low-chromium substitutes for heat-resisting stainless steels for the temperature range 600° to 800° C. Ferritic alloys are emphasized that have oxidation resistance provided by chromium contents as low as 10 pct and stress rupture strength provided by the precipitation of the chi(X)-phase intermetallic compound, ($Fe_{36}Cr_{12}$ (Mo, Ti)$_{10}$).

Initially, research was concentrated on selecting an alloy composition having a minimum chromium content with strengthening provided by the X-phase. An Fe-(10-12 pct)Cr-6 pct Mo-(1.5-2.0 pct)Ti alloy was selected.

After the alloy selection, the tensile, stress rupture, and oxidation properties were determined. Stress rupture properties were found to be similar to those of 304 stainless steel. However, the alloys possessed brittleness during both stress rupture and tensile testing, possibly as a result of too high a content of molybdenum and titanium. Higher than expected oxidation rates were found that may be caused by the high molybdenum content.

[1]Metallurgist, Albany Research Center, Bureau of Mines, Albany, OR.

INTRODUCTION

The Bureau of Mines is conducting research to find substitutes for alloys containing chromium as part of its effort to minimize the Nation's mineral needs through conservation and substitution. High-temperature (800° to 1,000° C) alloys and heat-resisting (600° to 800° C) stainless steels, critical to defense, aerospace, and other industries, require substantial chromium contents for which there are no known substitutes. The goal of this research has been to develop low-chromium substitutes for the heat-resisting stainless steels.

Heat-resisting alloys require resistance to both oxidation and stress rupture at elevated temperatures. In the heat-resisting austenitic stainless steels, oxidation resistance is provided by a high chromium content (18 to 25 pct); stress rupture resistance at elevated temperatures is provided by the austenitic structure, which is stabilized by a high nickel content (8 to 22 pct) and to a lesser extent by minor alloy constituents. Low chromium contents in the range of 9 to 12 pct can provide oxidation resistance for temperatures as high as 800° C (28).[2] However, such an alloy (without nickel and with a low carbon content) would have a ferritic structure that would be relatively weak at 600° to 800° C. Therefore, the approach of this research has been to utilize the 9 to 12 pct Cr content for oxidation resistance, and to provide strengthening to such a ferritic alloy by precipitation hardening.

Commercial ferritic heat-resisting alloys develop strength by solid-solution hardening with elements such as Cr, Mo, and V, and by the precipitation of carbides of these and other elements. Unfortunately, such strengthening mechanisms are most effective below 600° C. Precipitation hardening with second phases such as carbonitrides (22), nickel aluminides and titanides (12, 21), and copper compounds (22) are also limited above 600° C.

Alloys strengthened with the intermetallic compounds called the Laves phase, the R-phase, and the χ-phase have better stability above 600° C. Much research has been done on alloys precipitation hardened with Laves phases such as Fe_2Ti, Fe_2Ta, and Fe_2Mo (2-3, 8-10, 14, 16-17, 23, 26-27, 35, 37). To reduce the problems caused by swelling and embrittlement of austenitic stainless steels in nuclear reactors, the atomic energy agency of Belgium developed a ferritic stainless steel containing 13 pct Cr. This steel is precipitation hardened with a χ-phase having the formulation $Fe_{36}Cr_{12}Mo_3Ti_7$ (5, 20). Commercial maraging stainless steels with compositions Fe-(10-15 pct)Cr-(10-20 pct)Co-(3-6 pct)Mo utilize the precipitation of a combination of the Laves phase, the χ-phase, and the R-phase (an Fe-Cr-Mo-Co rhombohedral phase) for strengthening (6, 11, 24, 36).

Alloys precipitation hardened with the Laves phase and χ-phase intermetallic compounds have been the focus of Bureau of Mines research in this area. Initial research explored only the Laves phase strengthening mechanism (8-10), but after subsequent research showed that χ-phase alloys may be more stable at high temperatures, research into χ-phase alloys was included in the investigation. The goals of the χ-phase research were to identify a low-chromium alloy using χ-phase precipitation for hardening and to determine the properties of the alloy as a function of heat treatment. This report of investigations is the result of that research.

[2]Underlined numbers in parentheses refer to items in the list of references at the end of this report.

BACKGROUND

A knowledge of the complex four-component Fe-Cr-Mo-Ti system is essential for research on X-phase precipitation hardening alloys. The binary Fe-Mo and Fe-Ti diagrams (figs. 1-2) show that only the Laves or mu(μ)-phase (sometimes called an epsilon phase, ε) precipitates in these simple systems. Although the coexistence of both the Laves phase and the μ-phase in the Fe-Mo system is somewhat clouded (7, 16, 19, 32), the most current literature shows a Laves phase precipitating below about 950° C and a μ-phase precipitating at higher temperatures (32).

When chromium is added to these binary systems, the ternary systems Fe-Cr-Mo and Fe-Cr-Ti are formed (figs. 3-4). These systems have a ternary intermetallic compound called the X-phase. The X-phase has the α-Mn structure, and the chemical compositions are generally believed to be $Fe_{36}Cr_{12}Mo_{10}$ (15, 34) and $Fe_{36}Cr_{12}Ti_{10}$ (4, 33). In combining the two ternary systems to form the Fe-Cr-Mo-Ti quaternary system, there are indications that the X-phase has the composition $Fe_{36}Cr_{12}Mo_xTi_{10-x}$ (x = 0,1,2,...10), and that it is continuous in mixtures of the two ternary systems (29).

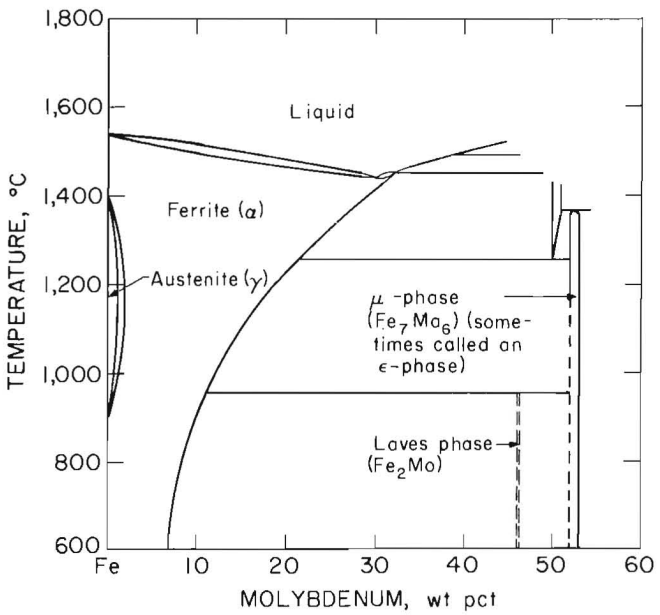

FIGURE 1. - Iron side of Fe-Mo phase diagram (18).

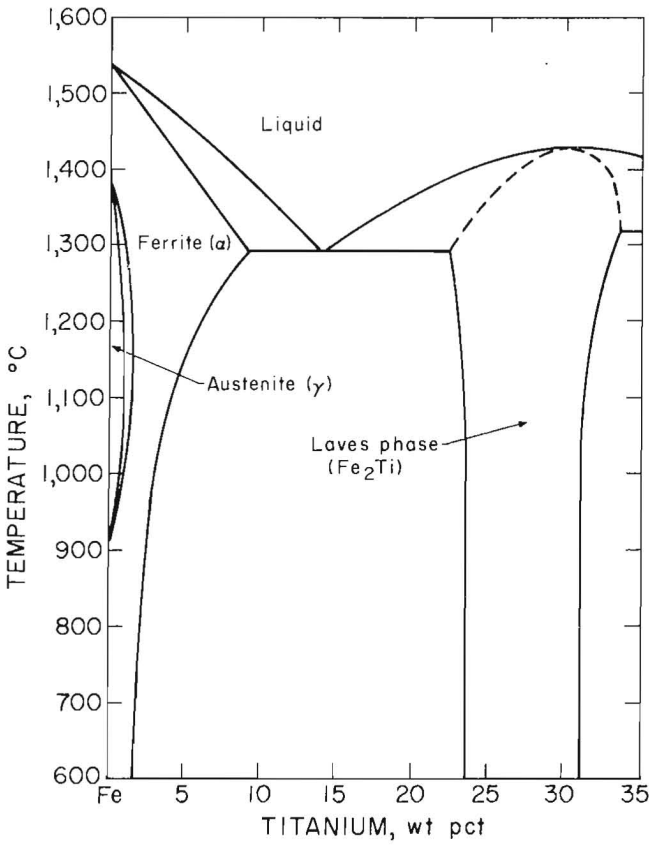

FIGURE 2. - Iron side of Fe-Ti phase diagram (31).

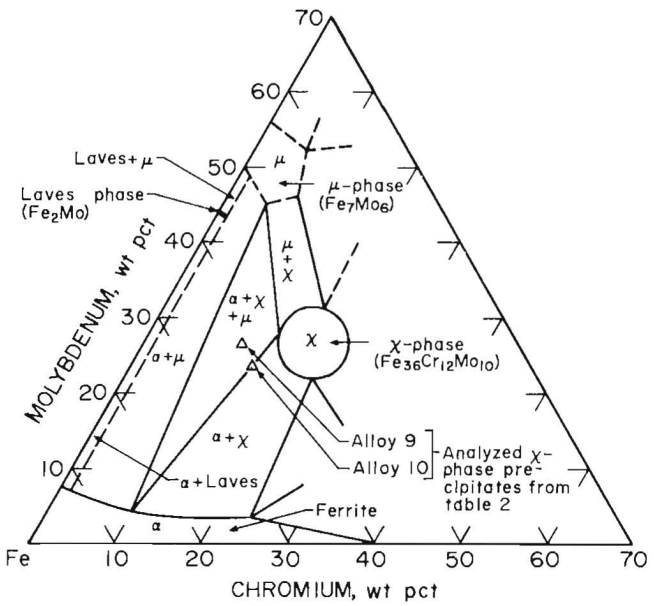

FIGURE 3. - 650° C isotherm from Fe-Cr-Mo ternary phase diagram (34).

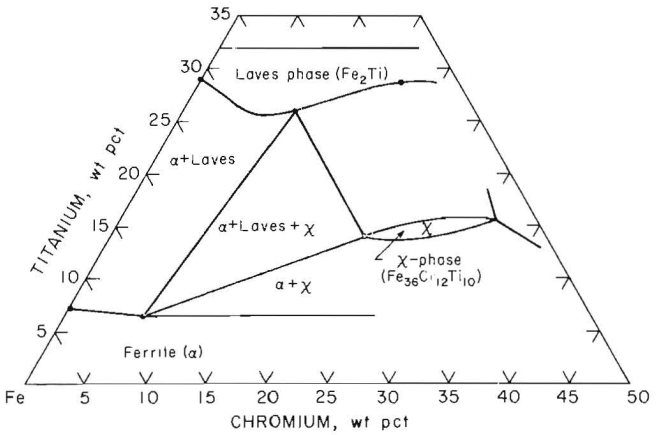

FIGURE 4. - 1,000° C isotherm from Fe-Cr-Ti ternary phase diagram (4).

Ternary or quaternary (Fe-Cr-Mo-Ti) alloys should be readily precipitation hardenable because the solubility of Cr, Mo, and Ti in Fe increases substantially with temperature. For aging of the precipitation hardenable alloys, the compositions of interest are in the multiphase regions, $\alpha + \chi$ or $\alpha + \chi$ + Laves. As the two ternary diagrams show, the $\alpha + \chi$ phase region occurs at about 10 pct Cr and above.

The Atomic Energy Agency of Belgium has developed a χ-phase alloy with the composition Fe-13Cr-3.5Ti-2Mo (5). Within a limited titanium and molybdenum range, Belgian scientists found that titanium was twice as effective as molybdenum for providing strength and decreasing ductility--probably a result of the difference in atomic weight. They found a drop in ductility from about 70 pct to zero when the combined Mo-Ti content, Ti + 0.5 Mo, reaches about 4.5 pct (5). Bureau of Mines research was concentrated on a combined Mo-Ti content that is balanced to provide both good strengthening and good ductility over a much broader range of compositions. To achieve the primary goal of developing a lower chromium, χ-phase alloy, it was necessary to determine how the minimum chromium content was affected by the molybdenum and titanium contents. The research was performed in two parts. Initially, small-scale (100-g) tests were used to select compositions for further investigation. Then, the properties of several larger, 10-lb (4.5-kg) ingots of the selected compositions were determined.

SELECTION OF ALLOY COMPOSITION

PROCEDURE

The 100-g test specimens were prepared by carefully weighing the following high-purity components:

Fe: Glidden A276 electrolytic iron.

Cr: Union Carbide Elchrome Regular electrolytic chromium.

Ti: Timet ML-115 titanium sponge.

Mo: Amax MMP molybdenum powder.

Samples were triple-arc-melted in helium atmosphere at 200-mm pressure and were homogenized for 20 h in a tungsten element vacuum furnace at 1,225° C and 10^{-4} Torr pressure. Chemical analyses of randomly selected samples were conducted to verify composition and are shown in table 1. Nominal compositions will be used throughout this report.

TABLE 1. - Chemical analysis of randomly selected alloys, weight percent

Nominal composition, wt pct	Cr	Mo	Ti
Fe-13Cr-4.5Ti.....	12.8	0	4.9
Fe-8Cr-6Mo-1.5Ti.....	8.2	6.1	1.3
Fe-13Cr-6Mo-1.5Ti.....	13.7	6.4	2.4
Fe-10Cr-10Mo.....	9.9	11.3	0
Fe-13Cr-5Mo-2Ti.....	13.0	5.2	1.4
Fe-10Cr-2Mo-3.5Ti.....	10.0	2.0	3.5
Fe-12Cr-2Mo-4Ti.....	11.9	2.1	5.0
Fe-12Cr-6Mo-2.5Ti.....	11.9	6.6	1.6
Fe-13Cr-6Mo-2.5Ti.....	12.7	6.0	1.5
Fe-12Cr-8Mo-1.5Ti.....	12.8	8.8	.9
Fe-12Cr-7Mo-2.5Ti.....	11.8	7.6	1.3
Fe-12Cr-10Mo-1.0Ti.....	11.9	10.6	.5
Fe-6Cr-6Mo-2Ti.....	5.9	6.6	1.1
Fe-10Cr-6Mo-2Ti.....	9.8	6.5	1.7

The 100-g alloys were forged and rolled at 1,100° C into bars approximately 1/8- by 3/4- by 8-in (3.2 by 19.1 by 203 mm). Specimens approximately 1 in (25.4 mm) long were cut from the rectangular bars and were encapsulated in quartz tubes backfilled with helium. The specimens were heated for 1 h at a nominal solution-treatment temperature of 1,250° C and quenched in boiling water. The solution-treated specimens were aged at 700° and 800° C for as long as 1,000 h. Room temperature Rhn A hardness measurements were made at various stages during the aging to provide a curve for the alloy. Metallographic examinations of the specimens after both short- and long-term exposures were performed to supplement the hardness data.

Supplementary data, including chemical analysis, electron microscopy, X-ray diffraction, and tensile tests, were obtained by standard techniques. To facilitate X-ray diffraction analysis of the strengthening phase, the precipitates were anodically extracted from many of the specimens. A dissolution cell, powered by a 15-V dc rectifier, was made using the alloy as the anode, a stainless steel cathode, and 50 gpL $FeCl_3$ solution. After 10 to 20 min of dissolution, the undissolved precipitates, released by the dissolving matrix, were filtered from the solution using a Millipore Filter[3] (25) and were analyzed by X-ray diffraction.

RESULTS

Effects of Molybdenum and Titanium on Ductility

An investigation of the effects of Mo and Ti on the tensile ductility of various Fe-12Cr-Mo-Ti alloys was completed using samples in the as-rolled condition. The ductility (percent reduction of area) is plotted on the ternary phase diagram in figure 5. These data agreed with Breyer's (5) conclusion that a rapid change from ductile to brittle failures results when Mo and Ti contents are increased beyond a certain maximum. However, the data show that the ductility limit occurs at a slightly lower combined Mo-Ti content than Breyer found for a 13-pct-Cr alloy for a narrower Mo-Ti range. Bend ductility tests of similar Fe-Mo-Ti alloys at Cr contents of 11 to 13 pct confirmed the above ductility limit and showed that the limit is not affected by the Cr level.

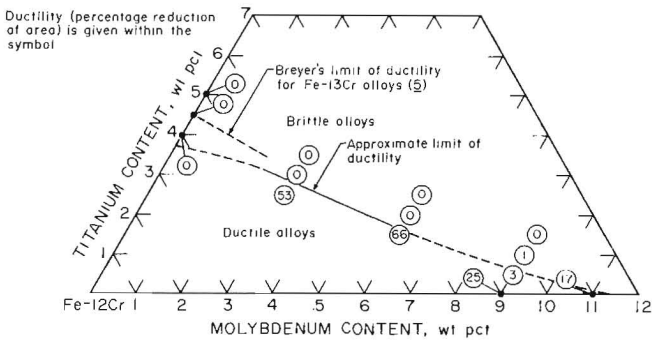

FIGURE 5. - Ductility of various Fe-12Cr-Mo-Ti alloys.

Precipitating Phases as a Function of the Chromium Content

Solution-treated alloy samples were aged at 700° and 800° C for as long as 1,000 h to determine their response to precipitation hardening. Aging at 700° C approximated our design conditions, while aging at 800° C indicated what might happen under longer term 700° C aging. Most of the alloys experienced an initial softening during the first hour of heating, probably a result of annealing or stress relieving. The subsequent aging curves were of three typical types for alloys with nominal compositions as shown in figure 6:

1. Continued hardening (fig. 6*A*)--These alloys show increasing hardness with time for both the 700° and 800° C tests.

2. Overaging (fig. 6*B*)--These alloys display an initial hardening followed by a softening at higher temperature and/or longer exposures.

[3]Reference to specific products does not imply endorsement by the Bureau of Mines.

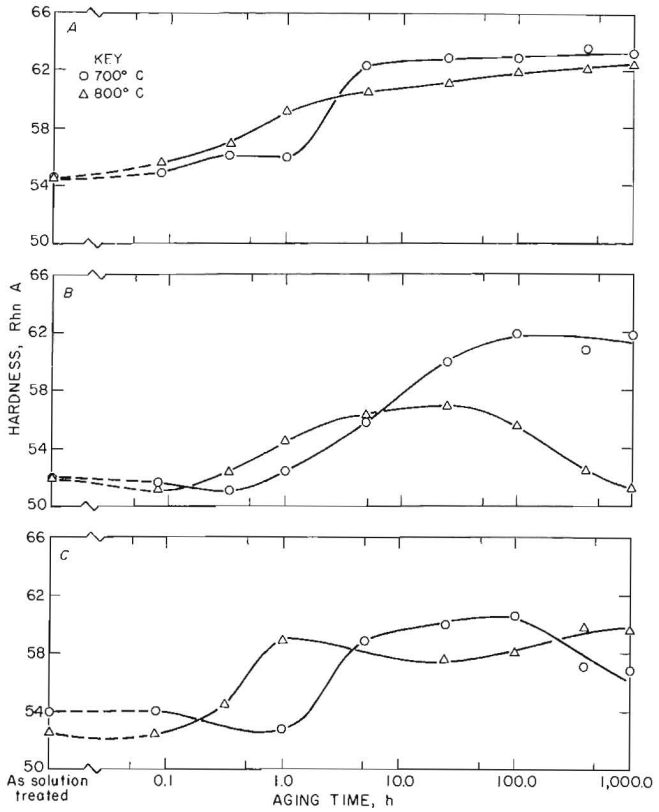

FIGURE 6. - Typical aging curves for Fe-Cr-Mo-Ti alloys. *A*, Continued-hardening curve for the Fe-12Cr-6Mo-2Ti alloy; *B*, overaging curve for the Fe-5Cr-6Mo-2Ti alloy; *C*, combined overaging and hardening curve for the Fe-10Cr-3Mo-3Ti alloy.

3. Combined overaging and hardening (fig. 6*C*)--These alloys show initial hardening followed by softening, similar to samples in figure 6*B*. At the higher temperature and for longer exposures, these alloys appear to increase in hardness again.

At a selected Mo and Ti content, the type of hardening appears to be affected by the Cr content. Continued hardening (fig. 6*A*) is typical of samples with higher chromium contents (9 to 15 pct Cr). Overaging (fig. 6*B*) occurs in samples with lower chromium contents (5 to 9 pct Cr). Combined overaging and hardening (fig. 6*C*) are observed at intermediate chromium contents (7 to 12 pct Cr). These changes in hardening response, shown here as a function of chromium content, indicate a change in the precipitation-hardening mechanism.

The change in hardening mechanism can be explained by a change in the precipitating phase. In fact, the Fe-Cr-Mo and Fe-Cr-Ti phase diagrams (figs. 3-4) show a transition from a Laves or μ second phase at chromium contents less than 10 pct to a X second phase at higher chromium contents. To determine whether this change in the precipitated phase correlates with the hardening data, a metallographic examination and several other analyses were conducted on the samples.

Photomicrographs of a given aged alloy at various levels of chromium content are shown in figure 7. At lower chromium contents, fine precipitates are observed; at higher chromium contents, coarse, blocky precipitates are seen; and at intermediate chromium contents, a mixture of coarse and fine precipitates is seen. These precipitates were anodically extracted from the specimens and analyzed by X-ray diffraction. The data, summarized in the last column of table 2, show that X-phase precipitates occur in the higher chromium content alloys and that a poorly crystallized phase occurs in the lower chromium content alloy. Therefore, we conclude that the differences in hardness curves at various chromium contents are caused by different precipitating phases. The overaging curves at lower chromium contents are probably a result of Laves phase precipitation, while the increased hardening curves at higher chromium contents are a result of the precipitation of the X-phase. The combined overaging and hardening at intermediate chromium levels is probably caused by the precipitation of a mixture of the two phases.

Precipitating Phases as a Function of the Molybdenum and Titanium Content

The Cr content at which the change in hardness mechanism occurs is affected by both the Mo and the Ti content. Molybdenum and titanium may be able to be substituted for each other because they occur in equivalent crystallographic positions in both the Laves phase and the X-phase. Furthermore, the ductility of

TABLE 2. - Electron microprobe and X-ray diffraction analysis of precipitates in various 800° C aged Fe-Cr-Mo-Ti alloys

Alloy	Nominal composition, wt pct	Composition of precipitates					
		Analysis by microprobe, at. pct					Structure by X-ray diffraction
		Fe	Cr	Mo	Ti	Mo+Ti	
1	Fe-10Cr-4.5Ti.....	Balance	13	0	13	13	X-phase, minor σ-phase.
2	Fe-12Cr-4.5Ti.....	Balance	14	0	13	13	X-phase.
3	Fe-10Cr-3Mo-3Ti.....	Balance	13	4	8	12	X-phase, trace others.
4	Fe-12Cr-3Mo-3Ti.....	Balance	15	4	9	13	X-phase.
5	Fe-7Cr-6Mo-1.5Ti....	Balance	10	10	6	16	X-phase, minor Laves and others.
6	Fe-10Cr-6Mo-1.5Ti...	Balance	14	9	5	14	X-phase.
7	Fe-12Cr-6Mo-1.5Ti...	Balance	16	8	5	13	X-phase, trace others.
8	Fe-7Cr-10Mo.....	Balance	7	33	0	33	Poorly crystallized (possibly Laves or σ-phase).
9	Fe-10Cr-10Mo.....	Balance	[1]14	[1]17	0	17	X-phase.
10	Fe-12Cr-10Mo.....	Balance	[1]17	[1]15	0	15	X-phase.
	Theoretical χ-phase, $Fe_{36}Cr_{12}(Mo,Ti)_{10}$.	62.1	20.7	NA	NA	17.2	
	Theoretical Laves phase, $Fe_2(Mo,Ti)$.	67	0	NA	NA	33	
	X-phase analysis by Okafor and Carlson (29).	72.1	15.3	NA	NA	12.6	

NA Not available. [1]Figure 3 shows data plotted on phase diagram.

Fe-Cr-Mo-Ti alloys is dependent on the combined Mo-Ti content, as discussed previously. Therefore, Fe-Cr-Mo-Ti alloys having a combined Mo-Ti content (pct Ti + pct Mo/2) that is close to Breyer's (5) limit of ductility were investigated in order to provide the best strengthening with adequate ductility. The hardening response of these alloys with several different Mo:Ti ratios was determined at Cr contents from 5 to 15 pct. The results are shown in figure 8. Continued-hardening curves, indicative of stable alloys, are found for the higher Cr alloys with all Mo:Ti ratios. However, when the alloy contains all Ti or all Mo, only alloys with the highest Cr content develop this stability. Stable alloys maintained at Cr contents as low as 10 pct are found at a balanced 6 pct Mo-1.5 pct Ti content.

The stabilities of alloys for a broader range of combined Ti-Mo content were also determined. The stabilities of some of these alloys are summarized in figure 9, which shows a 12-pct-Cr section through the Fe-Cr-Mo-Ti quaternary phase diagram. The stable zone depicted in the diagram encompasses the 6 pct Mo-1.5 pct Ti alloy mentioned in the previous paragraph. Fe-12Cr-Mo-Ti alloys outside this zone experience some overaging.

Microprobe Analysis of Precipitates

In addition to the X-ray diffraction of extracted precipitates, coarse precipitates in metallographic specimens were analyzed by the electron microprobe. The results, as shown in table 2, complement the X-ray diffraction data from the same samples. The analyses show that these X-phases average about 14 at. pct Cr and 14 at. pct (Mo + Ti), which is in good agreement with the data of Okafor and Carlson (29). For all the Mo:Ti ratios tested, the resulting total Mo + Ti content (at. pct) in the X-phase is fairly constant. This effect indicates that Mo

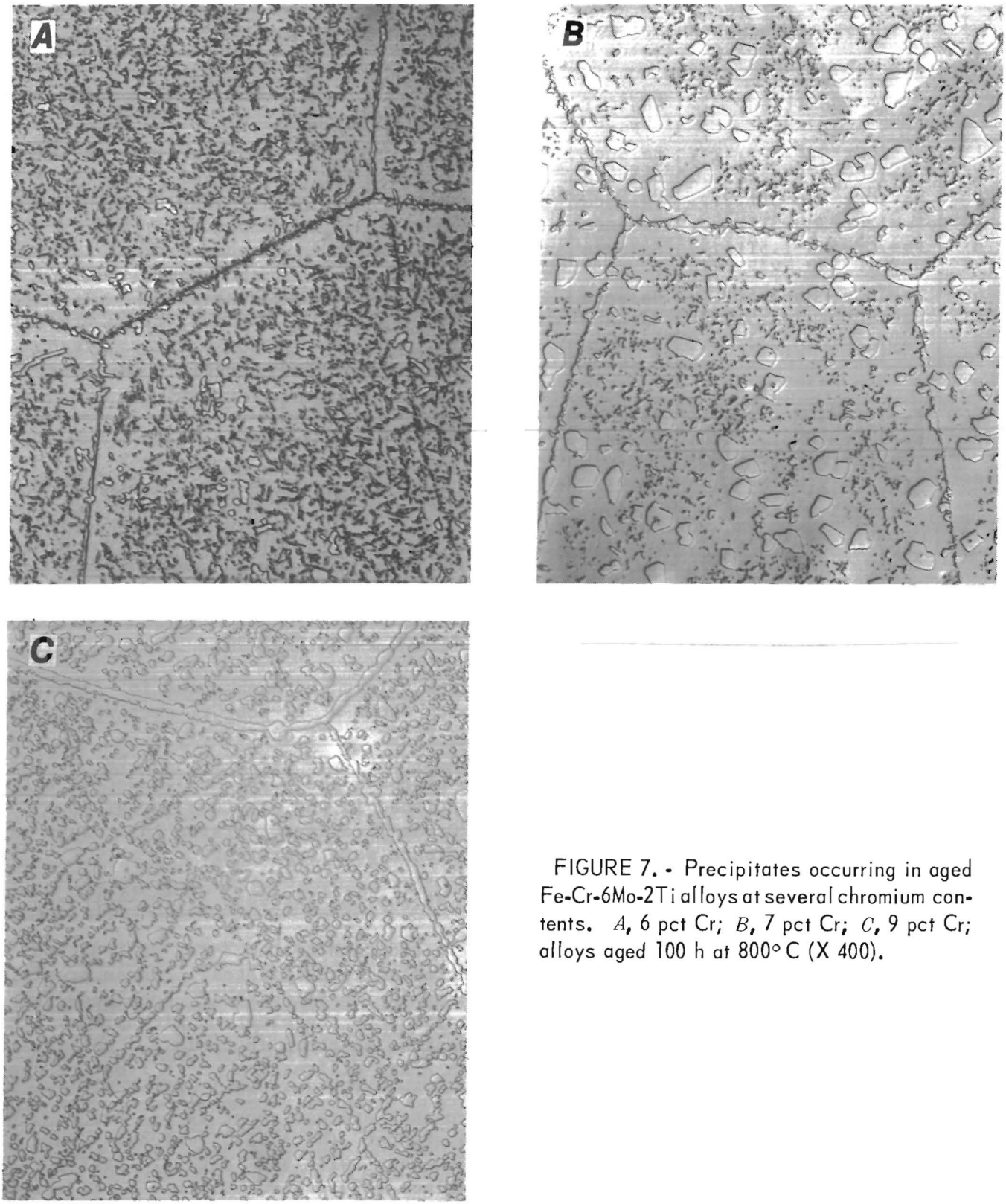

FIGURE 7. - Precipitates occurring in aged Fe-Cr-6Mo-2Ti alloys at several chromium contents. *A*, 6 pct Cr; *B*, 7 pct Cr; *C*, 9 pct Cr; alloys aged 100 h at 800° C (X 400).

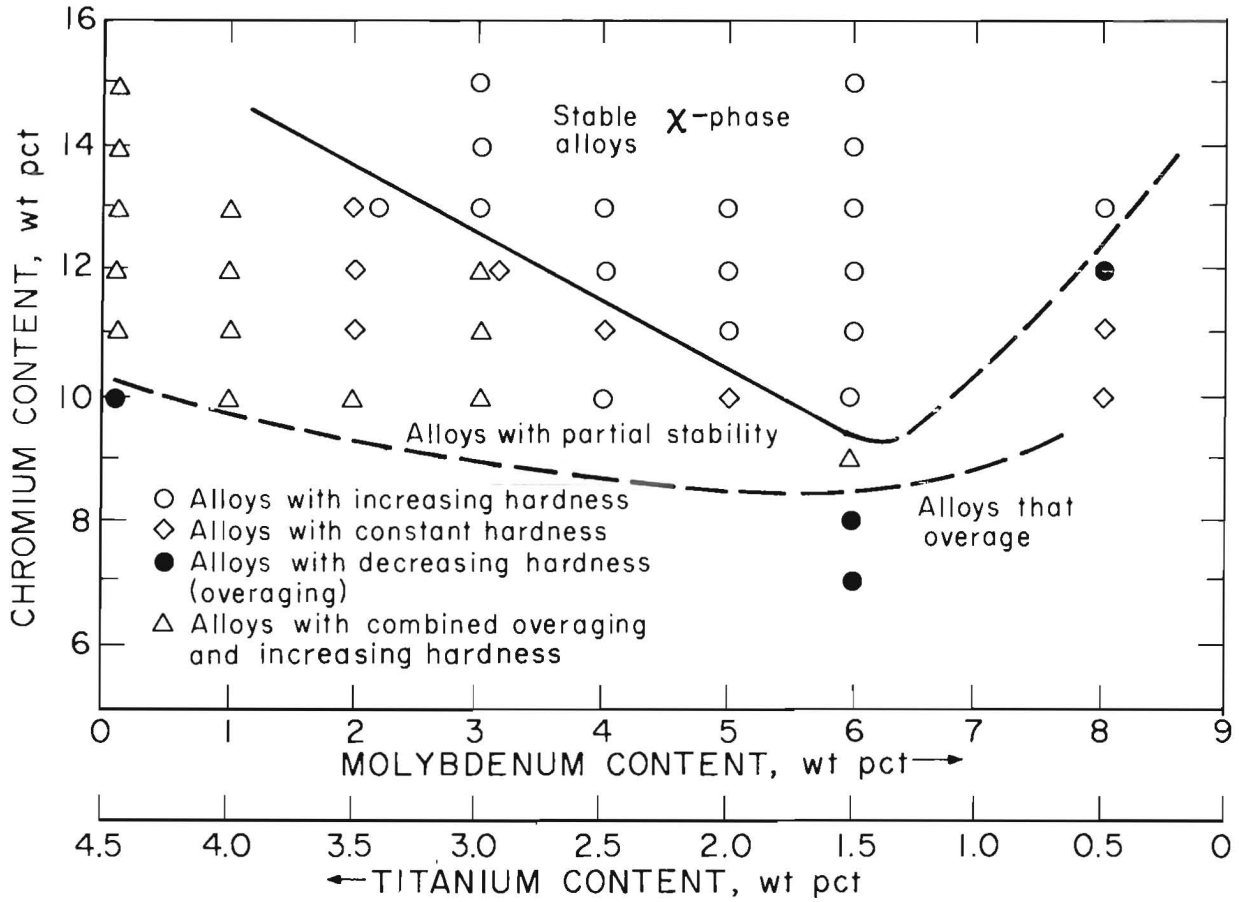

FIGURE 8. - Stability of various Fe-Cr alloys at combined Mo-Ti contents (pct Ti + pct Mo/2) of 4.5 pct. Alloys aged 1,000 h at 700° and 800° C.

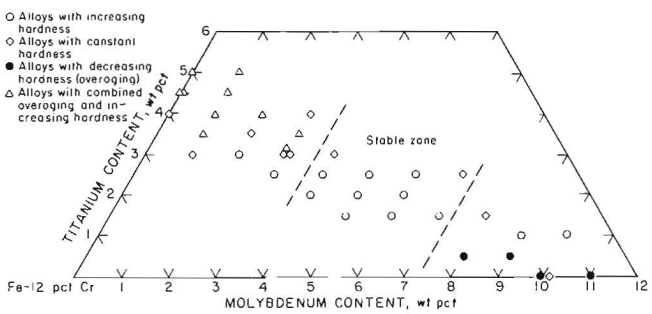

FIGURE 9. - Stabilities of Fe-12Cr-Mo-Ti alloys as a function of molybdenum and titanium content. Alloys aged 1,000 h at 700° and 800° C.

and Ti can substitute for or displace each other within the X-phase and suggests that there is a continuous X-phase field in combinations of the Fe-Cr-Mo and Fe-Cr-Ti phase diagrams. These analyzed compositions as well as the data of Okafor and Carlson (29) show the X-phase to be leaner in Cr, Mo, and Ti content than is shown in the Fe-Cr-Mo and Fe-Cr-Ti phase diagrams (figs. 3-4). For example, the weight percentage of the X-phase precipitates from alloys 9 and 10 in table 2 is plotted outside the X-phase region in figure 3. Apparently the X-phase has a much broader solubility range than is shown in these ternary phase diagrams.

DISCUSSION

The design of X-phase-strengthened alloys seems to be limited by several factors. First, sufficient Mo and Ti must be added to exceed the solubility limit to develop precipitation hardening. On the other hand, the Mo and Ti contents should be controlled to levels less than the ductility limit discussed previously.

The chromium content is also a constraining factor. Alloys with low chromium contents are subject to overaging

as a result of the precipitation of the Laves phase. Therefore, alloys need enough chromium to produce λ-phase precipitation hardening, but it is also desirable to conserve chromium. The chromium content necessary to minimize overaging is dependent on the Mo:Ti ratio. For example, Cr content as low as 10 pct can develop stable hardening at a composition of 6 pct Mo and 1.5 pct Ti.

Several alloy compositions were selected for further testing on a larger (10-lb) scale. To verify the ductility constraints on this scale, the compositions were selected near the ductility limit. Otherwise, the alloy compositions were designed around the above constraints. The selected alloys contained 10 to 12 pct Cr, 6 pct Mo, and 1.5 to 2.0 pct Ti.

PROPERTIES OF LOW-CHROMIUM λ-PHASE ALLOYS

PROCEDURE

The following nominal compositions were selected for large-scale testing:

Fe-10Cr-6Mo-1.5Ti Fe-10Cr-6Mo-2.0Ti

Fe-10Cr-6Mo-1.75Ti Fe-12Cr-6Mo-1.75Ti

Ten-lb (4.5-kg) cylindrical ingots were prepared from the same high-purity raw materials previously described and were melted in a vacuum-induction furnace. The ingots were scalped to approximately 2 in (51 mm) diam by 10 in (254 mm) length prior to fabrication. The chemical analysis of these alloys is shown in table 3. The ingots were homogenized in vacuum at 1,200° to 1,250° C for 20 h. The alloys were hot-worked at 1,100° C according to the following schedule with reheats between fabrication steps:

1. Upset forged (~20 pct hot worked).

2. Squared off in forge (~14 pct hot worked).

3. Rolled in 20-pct reductions to 1/2-in (12.7-mm) plate for stress rupture blanks and to 0.2-in (5-mm) plate for tensile test blanks.

Stress rupture and tensile test blanks were cut longitudinally from the rolled ingots. A 1,100° C solution treatment temperature was selected after examination for undissolved precipitates in specimens quenched from various temperatures. The resultant alloys had a coarse grain size of 0.3 to 0.5 mm, which should provide good stress rupture resistance. The blanks were heattreated by solution treating for 1 h at 1,100° C, followed by quenching in boiling water and by aging at 700° C. The blanks were machined into flat tensile specimens (1-in (25.4-mm) gage length with 0.250- by 0.120-in (6.4- by 3.1-mm) cross section) in accordance with ASTM specification E8-78 and into round stress rupture specimens (1-in (25.4-mm) gage length with 0.250-in (6.4-mm) diameter cross section) in accordance with ASTM specification E139-78. Tensile tests were conducted at room temperature at a 0.05-in/in·min^{-1} strain rate. Stress rupture tests were conducted at 700° C with a 1-h heatup and a 2-1/2-h stabilization time prior to loading.

To study the precipitation process, a density test of a similar alloy was conducted using the method of Rawlings and Newey (30). An Fe-13Cr-3Mo-3Ti alloy was vacuum-arc-melted for this test. After

TABLE 3. - Chemical analysis of ingots

Nominal composition, wt pct	Composition, wt pct			Composition, ppm		
	Cr	Mo	Ti	C	O	N
Fe-10Cr-6Mo-1.5Ti.....	10.0	6.2	1.7	NA	NA	NA
Fe-10Cr-6Mo-1.75Ti.....	10.2	6.2	1.9	61	375	70
Fe-10Cr-6Mo-2.0Ti.....	10.2	6.2	2.4	NA	NA	NA
Fe-12Cr-6Mo-1.75Ti.....	12.3	5.9	1.9	NA	NA	NA

NA Not available.

homogenization and fabrication similar to that described above, test samples were cut from the alloy, solution-treated at 1,100° C for 1 h, and water-quenched. Accurate density determinations (±0.001 g/cm^3) were made by the water-immersion technique by weighing to the nearest 0.1 mg. Determinations were made in triplicate after aging times ranging from 0 to 1,000 h for samples aged at 700° and 800° C. Comparative Rhn A hardness measurements were made on identical samples after the same heat treatments.

Oxidation tests of the Fe-10Cr-6Mo-1.75Ti and Fe-12Cr-6Mo-1.75Ti compositions were also completed at 700° and 800° C. Solution-treated samples approximately 3/4 in (19 mm) square by 0.2 in (5.1 mm) thick were cut and polished on a 120-grit belt sander and then measured to determine surface areas. After the samples were cleaned in soapy water, acetone, and alcohol, they were dried and weighed to the nearest 0.1 mg. After heating for various exposure times at 700° and 800° C, the samples were removed and weighed. The weight gain per surface area was calculated as a measure of the oxidation rate.

RESULTS

Room temperature tensile test results are summarized in table 4. The yield strengths are not available from some of the tests because an extensiometer was not always used, in anticipation of alloy brittleness and consequent instrument damage. The yield strength of these alloys appears to be affected by solid-solution hardening. The tensile strengths seem to be in accordance with the ductility; alloys having good ductility develop better tensile strength than do those with poor ductility. The ductilities were shown to vary considerably more than expected within the same alloy.

The stress rupture lives of these alloys in the solution-treated state shown in figure 10 are comparable to those of 304 stainless steel. The Fe-10Cr-6Mo-1.5Ti alloy (fig. 10*A*) has the best data fit for the stress rupture curves. Although the other three alloys have some data points showing stress rupture lives better than that of stainless steel, these alloys have considerable data variability, with some samples failing at much shorter periods than the rest of the samples. The fractured surfaces of specimens failing in short periods show a more brittle nature than do the surfaces of other specimens. The alloys that do not fail in a brittle manner have the best stress rupture lives.

TABLE 4. - Tensile data for solution-treated X-phase alloys

Nominal composition	Strength, psi		Ductility, pct	
	Yield	Tensile	Elongation	Reduction in area
Fe-10Cr-6Mo-1.5Ti.....	50,100	62,000	3	3
	51,400	71,200	8	6
	50,200	70,200	6	6
Fe-10Cr-6Mo-1.75Ti.....	NA	76,700	32	49
	52,400	70,800	7	7
	53,500	76,200	28	47
Fe-10Cr-6Mo-2Ti.....	NA	76,800	23	29
	NA	47,000	1	4
	NA	49,400	2	0
	NA	75,100	12	11
Fe-12Cr-6Mo-1.75Ti.....	54,700	77,800	16	13
	NA	64,600	4	2
	57,800	77,700	21	23

NA Not available.

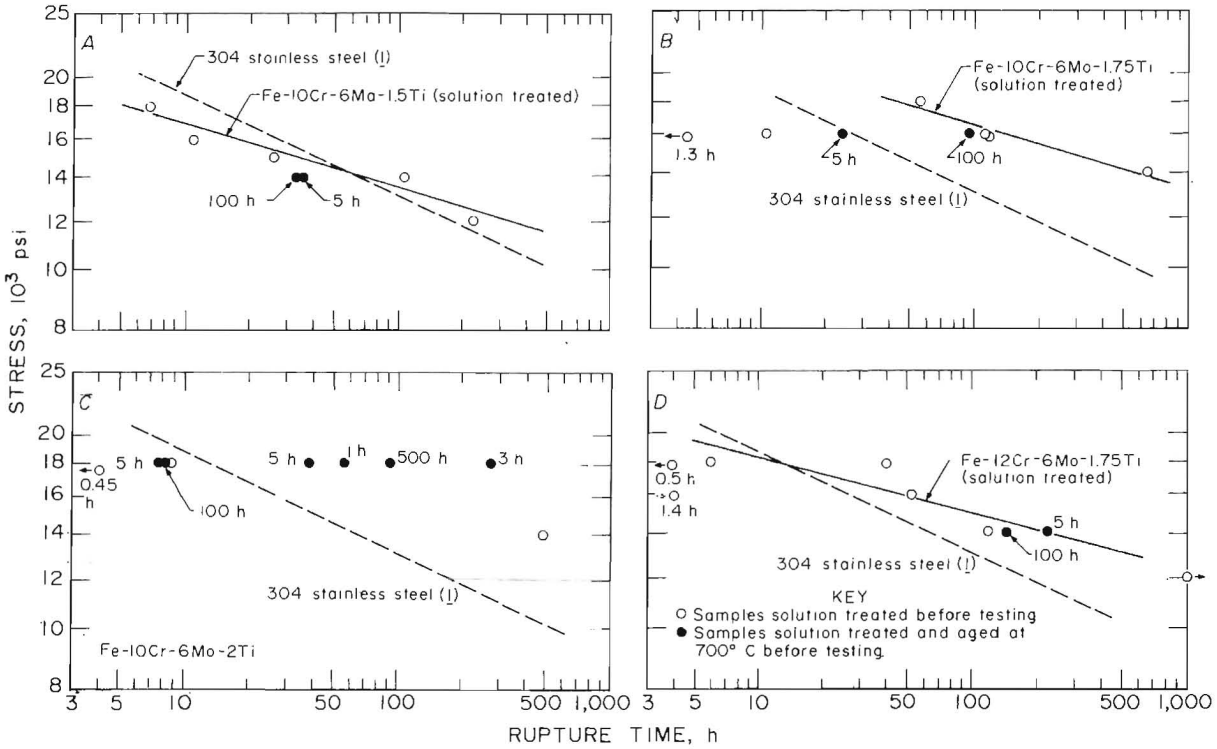

FIGURE 10. - Stress rupture curves for Fe-Cr-Mo-Ti alloys at 700° C. *A*, Fe-10Cr-6Mo-1.5Ti; *B*, Fe-10Cr-6Mo-1.75Ti; *C*, Fe-10Cr-6Mo-2Ti; *D*, Fe-12Cr-6Mo-1.75Ti.

The main purpose of the tests on the Fe-10Cr-6Mo-2Ti alloy was to determine the effects of aging on stress rupture life, but the data are so variable that no trend can be seen. However, these data, in conjunction with limited aging data for the other alloys, show that aging provides no benefit to stress rupture life.

As shown from both tensile tests and stress rupture tests, the results are quite variable because many alloys are brittle--much more than is usual in other ferritic alloys. Besides exhibiting brittle fracture surfaces, the tensile specimens frequently gave an audible "pop" during loading. Later examination showed many cracks throughout the specimen (fig. 11). Many of the stress rupture specimens also developed cracks that led to premature failure. Extremely brittle areas are typically found adjacent to very ductile areas, as is shown in figure 12. All the brittle failures were identified by SEM microscopy (fig. 13) to be of a cleavage, transgranular type with very little ductility. The

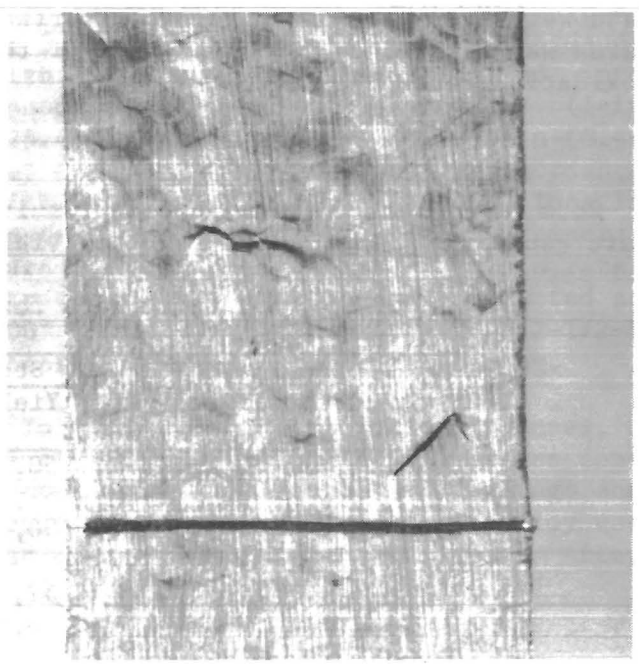

FIGURE 11. - Typical cracks that develop during loading of tensile specimens (X 10). Line at bottom is scribe mark for determination of elongation.

presence of this brittleness and the data variability indicate that these four alloys are at or beyond the ductile

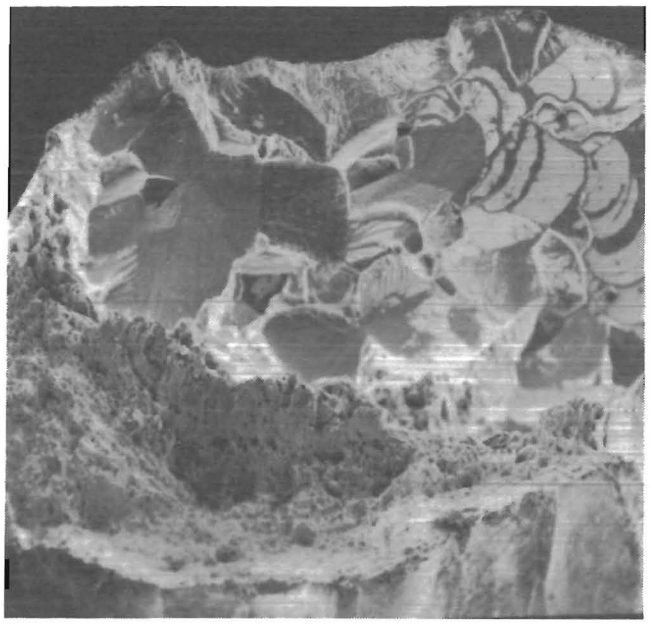

FIGURE 12. - SEM micrograph (X 25) showing ductile area (foreground) and brittle area (background) in an Fe-12Cr-6Mo-1.75Ti stress rupture specimen.

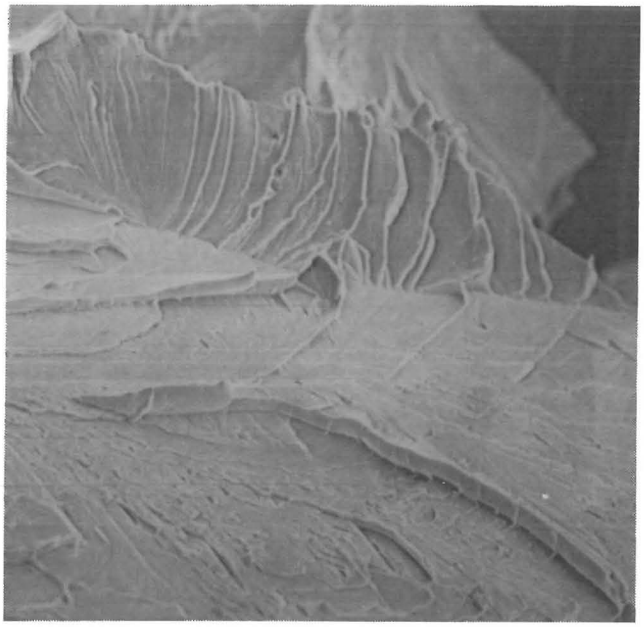

FIGURE 13. - SEM micrograph (X 640) of cleavage transgranular tensile test failure.

composition limit shown in figure 5. At this ductility limit, the ductility of an alloy can change from 66 pct to 0 pct with only a slight change in alloy content (1/2 pct for titanium). Therefore, the observed variation of ductilities and stress rupture lives is believed to be caused by slight compositional variations in this critical region. Metallographic examinations revealed no grain boundary precipitates or differences between ductile and brittle areas. Since these alloys possess more brittleness than is desired, future research should concentrate on alloys with lower molybdenum and titanium levels within the ductile region and away from the ductility limit.

The density tests of the similar Fe-13Cr-3Mo-3Ti alloy show insight into the precipitation mechanism. Density and the corresponding hardness changes for samples aged at 700° and 800° C are shown as a function of aging time in figure 14. Both the alloy density and hardness increase steadily with aging for as long as 1,000 h. Because density is a measure of the state of chemical equilibrium, the data indicate that precipitation of the second phase is very slow, taking 1,000 h or longer. The continued slow precipitation experienced here may explain why the hardness continues to increase even though very coarse precipitates, indicative of overaging, are present. Evidently fresh, newly formed submicroscopic precipitates being continually precipitated provide the hardening. Both the coarse and fine precipitates are probably the X-phase, but they were not identified.

The results of oxidation tests of the alloys, Fe-10Cr-6Mo-1.75Ti and Fe-12Cr-6Mo-1.75Ti, show oxidation rates higher than that of 304 stainless steel (18Cr-8Ni) at 700° C. The data for two separate oxidation tests shown in figure 15 exhibit an initial parabolic oxidation rate, which changes to a much higher rate after approximately 100 h. Overall, the rates are unpredictable for these alloys. For instance, the 10-pct-Cr alloy for the second test had an initial low parabolic oxidation rate followed by a relatively high oxidation rate; in the first test this 10-pct-Cr alloy gained weight at a relatively high oxidation rate throughout

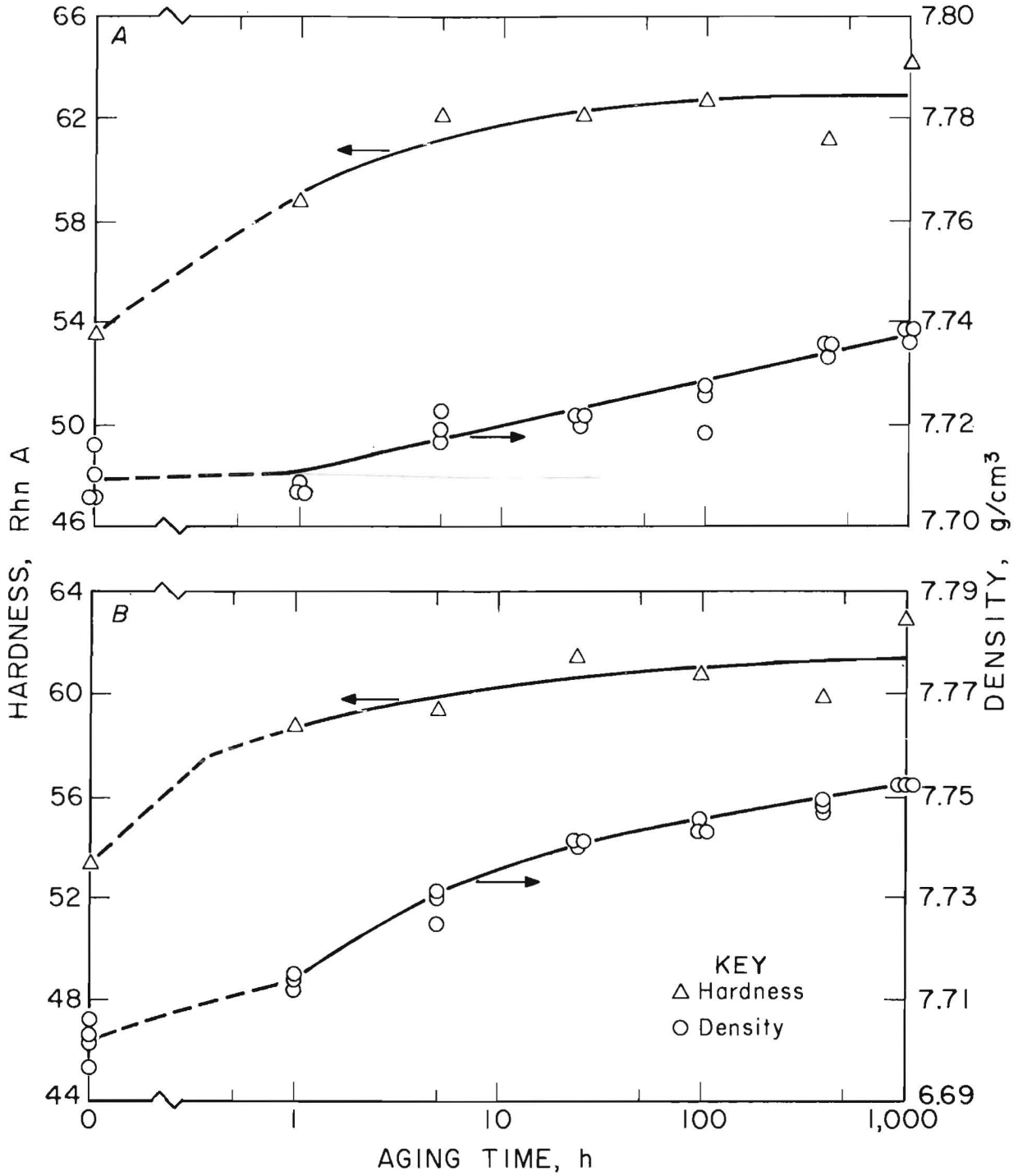

FIGURE 14. - Density and hardness changes during aging of an Fe-13Cr-3Mo-3Ti alloy. *A*, aging at 700° C; *B*, aging at 800° C.

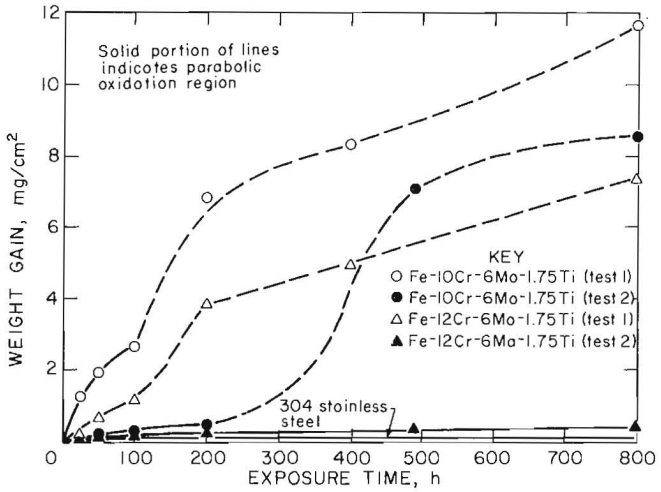

FIGURE 15. - Oxidation of χ-phase alloys at 700° C.

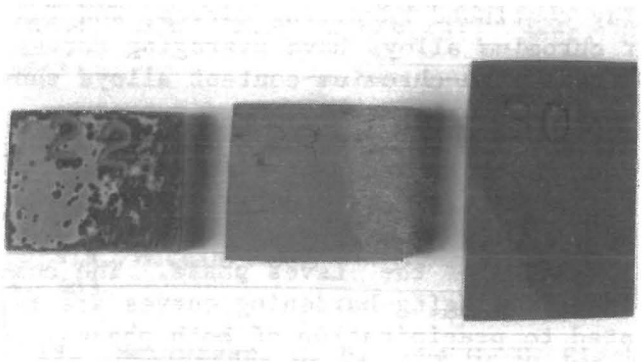

FIGURE 16. - Localized oxidation (X 1.5) of 10-pct-Cr alloy (sample 22, left) and 12-pct-Cr alloy (sample 23, middle) compared with oxidation of 304 stainless steel (sample 30, right). Exposed 800 h at 700° C.

the test. The 12-pct-Cr alloy had an extremely low oxidation rate throughout the second test, while it had a relatively high rate throughout the first test. The oxidation was also localized, as shown in figure 16. The metallographic cross section through the oxidized layer (fig. 17) also demonstrates the highly localized oxidation. Perhaps the localized nature of the oxidation explains the unpredictability of the oxidation results. Although iron-base alloys containing 10 or 12 pct Cr should be oxidation resistant at 700° C (28), alloys containing molybdenum have increased oxidation rates owing to a fluxing away of protective oxides by low-melting MoO_3 mixtures (13). Therefore the molybdenum content is believed to be the cause of the unexpectedly high, localized, and unpredictible oxidation rates. Since the alloy compositions tested do not provide sufficient oxidation resistance at 700° C, future research should include investigation of further enhancing oxidation resistance with aluminum additions.

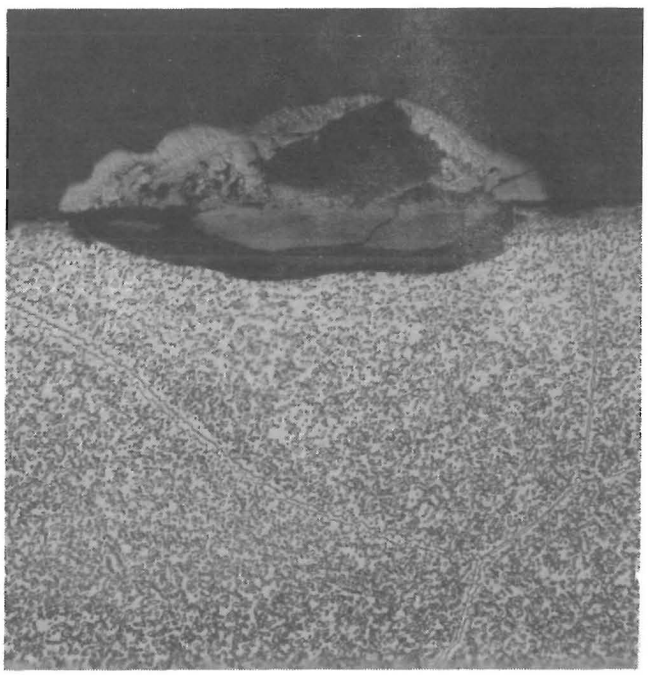

FIGURE 17. Cross section of localized oxidation (X 200) in Fe-12Cr-6Mo-1.75Ti alloy. Exposed 800 h at 700° C.

CONCLUSIONS AND RECOMMENDATIONS

The following conclusions are drawn from the alloy selection phase of the research.

1. Fractures in Fe-12Cr-Mo-Ti alloys rapidly change from a ductile to a brittle mode at increased titanium and molybdenum contents.

2. Three types of hardening curves were observed for these Fe-Cr-Mo-Ti alloys: (A) continued hardening curves, (B) overaging curves, and (C) combined overaging-hardening curves.

3. High-chromium-content alloys display continued hardening curves, and lower chromium alloys have overaging curves. Intermediate-chromium-content alloys show combined overaging-hardening curves.

4. Continued hardening curves are related to precipitation of the X-phase, and overaging curves are related to precipitation of the Laves phase. The combined overaging-hardening curves are related to precipitation of both phases.

5. The minimum chromium content at which continued hardening curves exist is dependent on the molybdenum and titanium contents. Continued hardening at a minimum of 10 pct Cr occurs at a composition of 6 pct Mo and 1.5 pct Ti.

The results of property studies of 10-lb ingots of Fe-(10-12)Cr-6Mo-(1.5-2.0)Ti alloys follow:

1. Stress rupture strengths of solution-treated alloys are comparable to that of 304 stainless steel at 700° C. Solution treating followed by aging provides no increase in rupture strength.

2. These alloys have a significant variation in ductility with considerable brittleness in both the tensile and stress rupture tests. The brittleness may be a result of too high molybdenum and titanium content.

3. The X-phase precipitation-hardening alloys continue to come to equilibrium after 1,000 h at both 700° and 800° C.

4. Oxidation resistance of these alloys at 700° C is poor owing to localized oxidation. This poor oxidation resistance may be a result of the high molybdenum content of the alloy.

To avoid the alloy brittleness problems observed in this research, it is recommended that future work be conducted on alloys with lower molybdenum and titanium contents. To minimize localized oxidation at 700° C, the addition of low levels of aluminum and/or silicon is recommended. The resolution of these brittleness and oxidation problems is necessary to develop a low-chromium substitute for the heat-resisting stainless steels.

REFERENCES

1. Air Force Materials Laboratory. Aerospace Structural Metals Handbook, FeA-1303. Syracuse Univ. Press, Syracuse, NY, rev. 1964, p. 16.

2. Bhandarkar, M. D., M. S. Bhat, E. R. Parker, and V. F. Zackay. Creep and Fracture of a Laves Phase Strengthened Ferritic Alloy. Met. Trans., v. 7A, May 1976, pp. 753-760.

3. Bhandarkar, M. D., M. S. Bhat, V. F. Zackay, and E. R. Parker. Structure and Elevated Temperature Properties of Carbon-Free Ferritic Alloys Strengthened by a Laves Phase. Met. Trans., v. 6A, June 1975, pp. 1281-1289.

4. Boroskina, N. G., and I. I. Kornilov. Isslyedovaniye Diagrammy Sostoyaniya Zhyelyeeo-Khrom-Titan V Oblasti Splavov Bogaykh Zhyelyeeom I Khromom. (Structural Diagram of Iron-Chromium-Titanium in the Area of Iron- and Titanium-Rich Alloys). Izv. Akad. Nauk SSSR, Otd. Tekh. Nauk, Metallurgiya i Toplivo, No. 1, 1960, pp. 50-58.

5. Breyer, J. P., J. M. Diez, V. Leroy, J. J. Huet, and L. Habraken. Ferritic Stainless Alloys Containing Titanium and Molybdenum as Major Alloying Additions. Metallurgical Reports C.R.M., No. 36, Sept. 1973, pp. 68-75.

6. Caton, R. L. A Maraging Stainless for 800° to 1,100° F Service. Metal Progress, v. 92, No. 1, 1967, pp. 106-108.

7. Coldren, A. P., M. Semchyshen, and W. G. Scholz. Factors Affecting the Strength of Iron-Rich Iron-Molybdenum-Boron Alloys. Trans. AIME, v. 230, 1964, pp. 1236-1250.

8. Dunning, J. S. Ferritic Iron-Based Alloys Strengthened by Laves Phase. Proc. 2d Internat. Conf. on Mechanical Behavior of Materials, ASM, Boston, Mass., Aug. 16-20, 1976, pp. 1832-1836.

9. ____. Iron-Based Alloys Strengthened by Ternary Laves Phases. BuMines RI 8411, 1980, 13 pp.

10. Dunning, J. S., M. L. Glenn, and W. L. O'Brien. Iron-Based Alloys Strengthened by Laves Phases as Substitutes for Stainless Steels. BuMines RI 8470, 1980, 24 pp.

11. Dyson, D. J., and S. R. Keown. A Study of Precipitation in a 12 pct Cr-Co-Mo Steel. Acta Metallurgica, v. 17, Aug. 1969, pp. 1095-1107.

12. Evans, D. G. The Development of Ferritic Steels Hardened by Intermetallic Compound Precipitation. Heat Treatment of Metals, v. 1, pt. 3, 1974, pp. 102-105.

13. Evans, U. R. Corrosion and Oxidation of Metals. St. Martin's Press, Inc., New York, 1960, p. 81-84.

14. Gemmill, M. G., H. Hughes, J. D. Murray, F. B. Pickering, and K. W. Andrews. Study of 7 Pct and 8 Pct Chromium Creep-Resisting Steels. J. Iron and Steel Inst., Oct. 1956, pp. 122-144.

15. Goldschmidt, H. J. Occurrence of the Beta-Manganese Structure in Transition Metal Alloys and Some Observations on Chi-Phase Equilibria. Metallurgia, July 1957, pp. 17-26.

16. Gorchakova, E. N., K. A. Lanskaya, and E. F. Yakovleva. Phase Composition of Heat-Resistant Ferritic and Austenitic Steels Precipitation-Hardened by Intermetallic Compounds. Metal Science and Heat Treatment, No. 3, Mar. 1969, pp. 180-184.

17. Hagel, W. C., F. A. Smidt, and M. K. Korenko (assigned to U.S. Energy Research and Development Administration, Washington, DC). High Strength Ferritic Alloy. U.S. Pat. 4,049,431, Sept. 20, 1977.

18. Hawkins, D. T. Phase Diagrams: Fe-Mo. In Metals Handbook: Metallography, Structure and Phase Diagrams, v. 8, ed. by T. Lyman. American Society for Metals, Metals Park, OH, 8th ed., 1973, p. 303.

19. Heijwegen, C. P., and G. D. Rieck. Determination of the Phase Diagram of the Mo-Fe System Using Diffusion Couples. J. Less-Common Metals, v. 37, 1974, pp. 115-121.

20. Huet, J. J., and V. Leroy. Dispersion-Strengthened Ferritic Steels as Fast-Reactor Structural Materials. Nuclear Technology, v. 24, Nov. 1974, pp. 216-224.

21. Irvine, K. J. The Development of High-Strength Steels. J. Iron and Steel Inst., v. 200, Oct. 1962, pp. 820-836.

22. ____. The Physical Metallurgy of Steel. J. Iron and Steel Inst., v. 207, June 1969, pp. 837-853.

23. Jones, R. H., E. R. Parker, and V. F. Zackay. Use of an Allotropic Phase Change To Enhance Ductility in Fe-Ta Alloys. Ch. in Electron Microscopy and Structure of Materials. Univ. CA Press, Berkeley, CA, 1972, pp. 829-838.

24. Kasak, A., V. K. Chandhok, and E. J. Dulis. Development of Precipitation Hardening Cr-Mo-Co Stainless Steels. Trans. ASM, v. 56, 1963, pp. 455-467.

25. Koh, P. K. Occurrence of Chi-Phase in Molybdenum-Bearing Stainless Steels. Journal of Metals, v. 5, Feb. 1953, pp. 339-343.

26. Koutsky, J. Influence of Niobium, Titanium, and Boron on High-Temperature Properties of 12 Pct Cr-2 Pct W-V Steel. J. Iron and Steel Inst., v. 205, July 1967, pp. 763-768.

27. Koutsky, J., and J. Jezek. Composition of Precipitates in Modified 12 Pct Chromium Steels in the Range Above 550° C. J. Iron and Steel Inst., v. 200, Nov. 1962, pp. 938-943.

28. National Materials Advisory Board. Contingency Plans for Chromium Utilization. Nat. Acad. Sci., Washington, DC, NMAB-335, 1978, p. 77.

29. Okafor, I.C.I., and O. N. Carlson. Equilibrium Studies on a Chi Phase-Strengthened Ferritic Alloy. Met. Trans. A, v. 9A, Nov. 1978, pp. 1651-1657.

30. Rawlings, R. D., and C. W. Newey. The Aging Characteristics of an Fe-11 At-Pct Mo Alloy. Trans. of Met. Soc. of AIME, v. 242, 1968, pp. 1001-1007.

31. Rohatgi, P. K. Phase Diagrams: Fe-Ti. In Metals Handbook: Metallography, Structure and Phase Diagrams, v. 8, ed. by T. Lyman. American Society for Metals, Metals Park, OH, 8th ed., 1973, p. 307.

32. Sinha, A. K., R. A. Buckley, and W. Hume-Rothery. Equilibrium Diagram of the Iron-Molybdenum System. J. Iron and Steel Inst., v. 205, pt. 2, Feb. 1967, pp. 191-195.

33. Snykers, M., R. Serneels, P. Delavignette, R. Gevers, and S. Amelinckx. Inversion Domains in the X-Phase Alloy $Fe_{36}Cr_{22-x}Ti_x$ with $8 < x < 10$. Crystal Lattice Defects, v. 3, 1972, pp. 99-101.

34. Wada, T. Phase Diagrams: Cr-Fe-Mo. In Metals Handbook: Metallography, Structure and Phase Diagams, v. 8, ed. by T. Lyman. American Society for Metals, Metals Park, OH, 8th ed., 1973, p. 421.

35. Wert, J. A. Fundamental Investigation of Continuous Precipitation in an Fe-Nb Creep Resistant Alloy. D. Sc. Thesis, Univ. CA, Berkeley, CA, 1979, 135 pp.

36. West, D. R. F. The Constitution of Iron-Rich Alloys of the Fe-Cr-Co-Mo System; A Review. Cobalt, v. 51, June 1971, pp. 77-90.

37. Zackay, V. F., E. F. Parker, and D. Bhandarkar. The Structure and Properties of a Non-Carbon-Containing BCC Iron Alloy at Room and Elevated Temperature. Paper in Rate Processes in Plastic Deformation of Materials (Proceedings from John Dorn Symposium 1972). American Society for Metals, Metals Park, OH, 1975, pp. 542-559.

☆U.S. GPO: 1984-705-020/5010

INT.-BU.OF MINES,PGH.,PA. 27394